

Manipulating Giant Rashba Valley Splitting and Quantum Hall States in Few-Layer Black Arsenic by Electrostatic Gating

Feng Sheng,^{1,*} Chenqiang Hua,^{1,*} Xikang Sun,¹ Jie Hu,¹ Qian Tao,¹ Hengzhe Lu,¹ Yunhao Lu,¹ Mianzeng Zhong,² Kenji Watanabe,³ Takashi Taniguchi,³ Qinling Xia,^{2,†} Zhu-An Xu,^{1,4,‡} and Yi Zheng^{1,4,§}

¹*Zhejiang Province Key Laboratory of Quantum Technology and Device,
Department of Physics, Zhejiang University, Hangzhou 310027, P. R. China*

²*School of Physics and Electronics, Hunan Key Laboratory for Super-microstructure and Ultrafast Process,
Central South University, Changsha 410083, P. R. China*

³*National Institute for Materials Science, 1-1 Namiki, Tsukuba, 305-0044, Japan*

⁴*Collaborative Innovation Centre of Advanced Microstructures,
Nanjing University, Nanjing 210093, P. R. China*

(Dated: October 27, 2020)

Exciting phenomena may emerge in non-centrosymmetric two-dimensional (2D) electronic systems when spin-orbit coupling (SOC) interplays dynamically with Coulomb interactions, band topology, and external modulating forces, etc [1–5]. Here, we report illuminating synergetic effects between SOC and Stark in centrosymmetric few-layer black arsenic (BAs), manifested as giant Rashba valley splitting and exotic quantum Hall states (QHS) reversibly controlled by electrostatic gating. The unusual finding is rooted in the puckering square lattice of BAs, in which heavy $4p$ orbitals form highly asymmetric Γ valley with the p_z symmetry and D valleys of the p_x origin, located at the Brillouin zone (BZ) center and near the time reversal invariant momenta of X , respectively. When the structure inversion symmetry is broken by perpendicular electric field, giant Rashba SOC is activated for the p_x bands to produce strong spin-polarized D^+ and D^- valleys related by time-reversal symmetry, coexisting with weak Γ Rashba bands constrained by the p_z symmetry. Intriguingly, strong Stark effect shows the same p_x -orbital selectiveness for D , collectively shifting the valence band maximum of D^\pm valleys to exceed the Γ pockets. Such an orchestrating effect between SOC and Stark allows us to realize gate-tunable spin valley manipulations for 2D hole gas, as revealed by unconventional magnetic field triggered *even-to-odd* transitions in QHS. For electron doping, the quantization of the Γ Rashba bands is characterized by peculiar density-dependent transitions in band topology from two parabolic valleys to a unique inner-outer helical structure when charge carrier concentrations increase.

The coupling of electron spin and orbit degrees of freedom is one of the most profound effects in crystals, playing as the foundation of various fascinating phenomena, such as antisymmetric Dzyaloshinskii-Moriya exchange interaction [1], magnetoelectric coupling [2], topological quantum states [3], and the celebrated Dresselhaus and Rashba splitting in energy bands [4]. To activate such spin-orbit coupling (SOC), a lack of spatial inversion center is a necessity, by breaking either bulk- or structure inversion symmetry of crystal lattices. The emergence of van der Waals (vdW) crystals in recent years opens unprecedented opportunities in exploring SOC physics in the two-dimensional (2D) limit [5, 6], when the coupling is tuned by atomic-precision control of quantum confinement and by external modulation of electric field, charge doping and/or vdW heterostructure.

Here, we report the discovery of gate-tunable giant Rashba valley splitting with spin-valley flavors and unconventional quantum Hall states in few-layer black arsenic, via synergetic SOC and Stark effects with the

same orbital geometry selectivity. Black arsenic (BAs) is the group-V analogue of the renowned black phosphorus (BP) [7, 8], sharing the same centrosymmetric square lattice in which puckered monolayers are AB-stacked along the c axis (Figure 1a). The driven force to form such a puckered square lattice, symbolized by highly anisotropic *zigzag* and *armchair* crystallographic axes, is resonant bonding of orthogonal p orbitals to satisfy the condition of half-filled bands [9, 10]. The resulting semiconductors have rather unique electronic structure with p -orbitals dominating both valence band (VB) and conduction band (CB), showing multiple valleys with distinct p -orbital symmetry (Fig. 1b). Explicitly, for all BP-type materials, the VB maximum (VBM) and CB minimum (CBM) at the Brillouin zone center (designated as Γ valley) are predominated by p_z orbitals, while p_x orbitals form another set of band extremums along the $\Gamma - X$ directions, *i.e.* doubly degenerate D valleys enforced by inversion symmetry (IS) and time reversal symmetry (TRS). Intriguingly, the relative VBM energy between Γ and D valleys are determined by the strength of sp -hybridization. For BP, substantial $3s3p$ hybridization pushes the anti-bonding VBM of the Γ valleys far above the D -valley top, producing the well-known zone-centered direct band gap. For BAs, $4s4p$ hybridization is much weaker than BP, resulting in very close VBM energy between D and Γ valleys (~ 0.2

* Equal contributions

† qlxia@csu.edu.cn

‡ Zhuan@zju.edu.cn

§ Correspondence and requests for materials should be addressed to Y.Z. (email: phyzhengyi@zju.edu.cn)

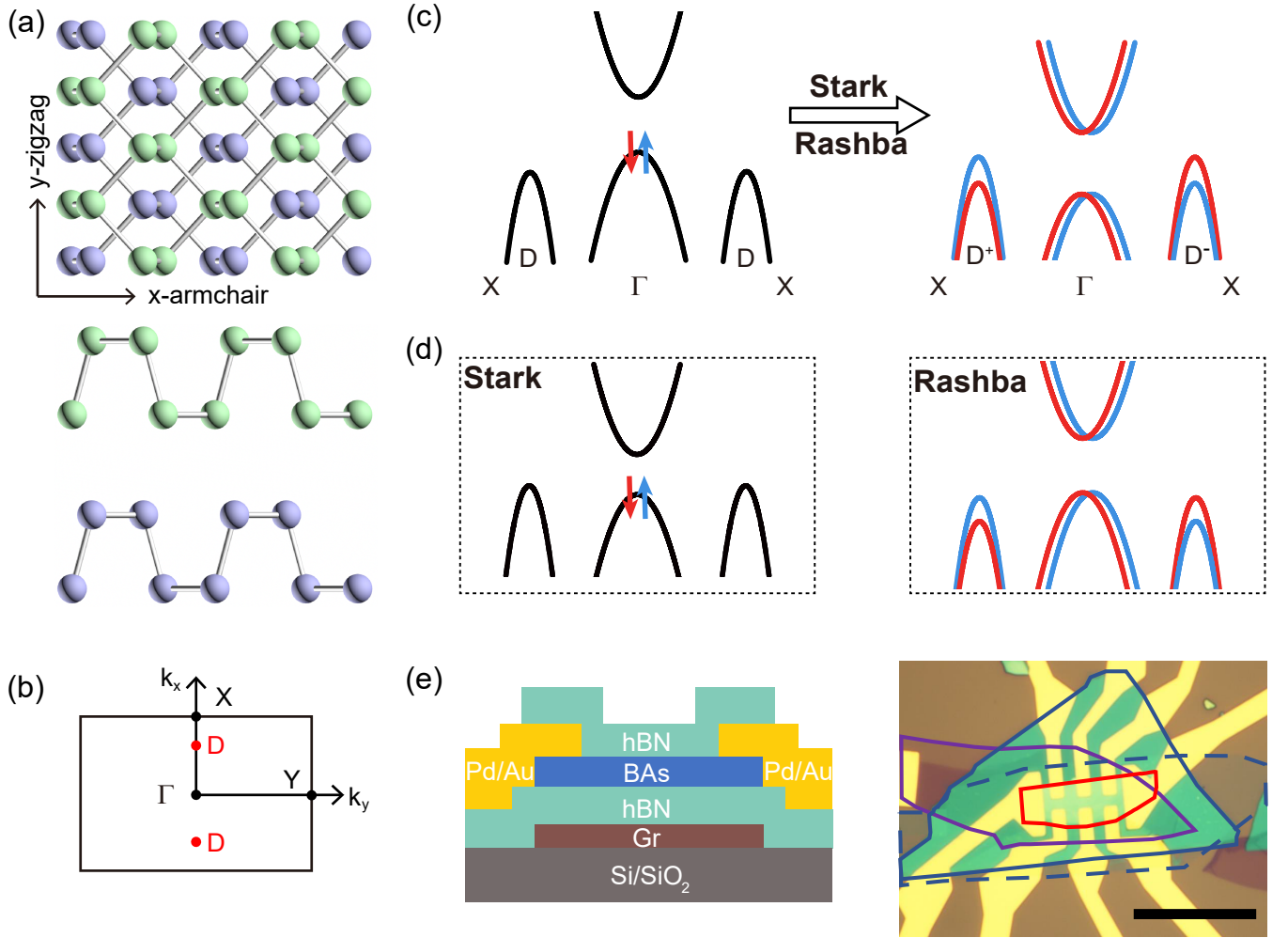


Figure 1. Gate-tunable giant Rashba valley splitting in BAs by synergetic Rashba and Stark effects. **a**, Top and side views of BAs crystal structure. BAs monolayers are AB stacked, while in the vdW plane, the puckering square lattice forms distinctive zigzag and armchair edges. **b**, The first Brillouin zone of BAs. Unlike BP, the degenerate D valleys in BAs are only 0.2 eV lower in VBM energy than the Γ valley. **c**, Energy bands' evolution of BAs with synergetic Stark effect and Rashba SOC under E_z , which create spin-polarized D^\pm valleys with higher VBM energy than Γ . **d**, Energy bands of BAs under Stark effect (left panel) or Rashba SOC (right panel) only. **e**, Left Panel: Schematic cross section diagram of hBN/BAs/hBN/graphite devices. Right Panel: Optical image of a BAs FET, in which BAs channel and graphite V_g are outlined by red and purple lines, while the top and bottom hBN layers are indicated by solid and dashed blue lines respectively. The scale bar is 20 μm .

eV), as demonstrated by angle-resolved photoemission experiments [11]. Note that for binary BP of SnSe, sp -hybridization is negligible and the Γ -valley VBM is well below the D valleys, which form an indirect band gap with the Γ -valley CBM [12].

We now elucidate the synergetic effects between SOC and Stark with the same p_x -orbital selectivity, which is the key to realize reversible control of spin-valley flavored Rashba valley splitting in BAs (Fig. 1c). It is known that the quantization of few-layer BP in high magnetic field above 30 T is prevailed by Zeeman effect [13], while SOC is negligible due to light atomic weight of phosphorus element. One period larger than P, As has considerable SOC of 0.43 eV [14], which can induce large energy band splitting when out-of-plane electric field breaks the

structure inversion symmetry, *i.e.* extrinsic Rashba effect. Qualitatively, such external electric field induced band splitting can be described by,

$$\hat{H}_R = \frac{\alpha_R}{\hbar} \boldsymbol{\sigma} \cdot (\mathbf{E}_z \times \mathbf{p}) \quad (1)$$

in which α_R , $\boldsymbol{\sigma}$, \mathbf{E}_z , and \mathbf{p} are Rashba parameter, Pauli spin matrices, perpendicular electric field, and momentum, respectively. From this formula, we can already see the orbital selectiveness of \mathbf{E}_z -induced SOC band splitting, which is small for the Γ valley due to p_z symmetry but becomes maximized for the D bands with large p_x momenta in the vicinity of time reversal invariant momenta (TRIM) of X . By activating Rashba SOC, the D valleys become spin-valley polarized as designated by \pm flavors, representing the product of spin (σ_z) and valley

(τ_z) indexes for the top spin channel of each D valley respectively (Fig. 1c). Such flavor-dependent Rashba band splitting of D^\pm is centering on TRIM points of X , distinct from the well-known Γ -centered Rashba effect in BiTeI [4, 15, 16].

On the other hand, BP shows giant Stark effect (GSE) [17, 18], which can even completely close the band gap by heavy electron doping [19]. External electric field also induces GSE in BAs, where a profound orbital selectivity for p_x -bands emerges to push the VBM of the D valleys above Γ (Fig. 1d). The different response of the Γ and D^\pm valleys to \mathbf{E}_z represent a larger GSE coefficient for the latter [see Note 1 in Supplementary Information (SI) for detailed discussions]. Similar orbital-dependent GSE has been systematically explored for transition metal dichalcogenides (TMDCs), which reveal that \mathbf{E}_z weakens interlayer coupling by depleting p_z orbitals and redistributing charges into the vdW planes [20]. The collective p_x -orbital selectivity for SOC and Stark effects causes drastic VBM reconstruction when the spin-polarized D^\pm valleys gradually take over the Γ valley as \mathbf{E}_z increases, making the reversible control of giant flavor-dependent Rashba valley splitting in BAs feasible (see schematic in Fig. 1c). Using temperature(T)- and angle(θ)-dependent magneto transport, we probe the quantum signatures of such reversible Rashba valley splitting, which manifests as exotic *even-to-odd* transitions in quantum Hall states when Fermi level (E_F) is crossing two sets of unconventional spin-valley asymmetric Landau levels and moving towards the massive Dirac points of the D^\pm valleys.

Figure 1e shows the typical device structure of BAs thin-film field-effect transistors (FETs). BAs flakes were micro-mechanically exfoliated from natural single crystals [11, 21, 22] in a glovebox with argon atmosphere. BAs layer thickness (10 – 25 nm) were estimated by optical contrast and ultimately determined by non-contact atomic force microscopy (see SI Note 2). Compared to BP, BAs micro-flakes exhibit impressive air stability, as evident by robust and repeatable Raman spectroscopy over tens of hours of ambient exposure. Nevertheless, for quantum transport measurements, device protection and isolation from the underlying SiO₂ substrate are decisive to observe the intrinsic quantization behavior of BAs. To achieve this, we encapsulated BAs FETs between two hexagonal boron nitride (hBN) layers while an extra graphite layer was lying at the bottom to serve as the back gate (V_g), a device structure used for studying quantum Hall effects (QHE) in BP [13, 23]. The hBN flakes effectively isolate BAs FET channels from ambient exposure, and the bottom hBN (~ 20 nm) is slightly thicker than the top one (~ 5 nm) since the former also serves as the dielectric layer for the back gate ($\sim 3 - 5$ nm).

The high quality of our BAs devices were evident by excellent field effect transfer characteristics (see Figure 2a and SI Note 3). As a function of V_g , BAs FETs show ambipolar transitions from electron to hole conduction for positive and negative gate bias respectively (inset of Fig-

ure 2a). Using Pd/Au contacts, we can readily achieve Hall mobility (μ_H) exceeding $5000 \text{ cm}^2\text{V}^{-1}\text{s}^{-1}$ for both 2D electron gas (2DEG) and hole gas (2DHG) at 1.6 K, which is truly remarkable and comparable to the best quality BP 2DHG. In the following, we show consistent results from two representative BAs FETs, with rather different hole μ_H of 1600 (BAs-S2) and $5100 \text{ cm}^2\text{V}^{-1}\text{s}^{-1}$ (BAs-S9) respectively. Similar to BP, BAs exhibits T -dependent μ_H , which becomes saturating below 30 K (Figure 2a). Typically, when T is lowered from 300 K to 1.6 K, μ_H increases from about $100 \text{ cm}^2\text{V}^{-1}\text{s}^{-1}$ to $5000 \text{ cm}^2\text{V}^{-1}\text{s}^{-1}$ for both hole and electron doping. Figure 2a also demonstrates the wide tunability of carrier densities in the range of $1 - 8 \times 10^{12} \text{ cm}^{-2}$, which is linearly proportional to V_g at $T = 0.27$ K. The increase in μ_H in response to carrier density accumulation suggests that disorder scattering correlated to residual impurities in BAs can be effectively screened by mobile carriers, in agreement with high quality BP devices [13, 24].

With the extraordinary carrier mobility of our BAs devices, we are able to observe fascinating Shubnikov-de Haas (SdH) oscillations in the magnetoresistance R_{xx} and exotic quantum Hall states (QHS) transitions in the Hall resistance R_{xy} for gate-tunable Rashba valley formation with unusual flavor dependence, the very first report among 2D materials to the best of our knowledge. As shown in Fig. 2b and 2c for the ambipolar BAs-S9 FET, robust SdH peaks emerge at low magnetic field (B) below 2 T for both 2DEG and 2DHG at 0.27 K. Using the empirical formula $\mu \sim 1/B_c$, we deduce an equivalent carrier mobility of $\sim 5000 \text{ cm}^2\text{V}^{-1}\text{s}^{-1}$, in good agreement with the Hall results. Much to our surprise, well-defined QHS with an astonishing maximum filling factor (ν) of 58 develop in R_{xy} for 2DHG of $5.30 \times 10^{12} \text{ cm}^{-2}$, accompanying SdH minima precisely. By plotting R_{xx} and R_{xy} together, it is conspicuous to see a pronounced field-dependent transition in the SdH oscillations from even- ν QHS sequences to odd- ν QHS plateaus. However, with a lower hole doping of $2.94 \times 10^{12} \text{ cm}^{-2}$, SdH oscillations of 2DHG start with odd- ν QHS directly (see SI Note 4 and 5 for more details). For both cases, Zeeman splitting induced double peaks become distinctive features in R_{xx} for B above 6 T, where the local double-peak minima correspond to kinks instead of well-developed plateaus in R_{xy} . In stark contrast, SdH oscillations of 2DEG have drastically different quantization behavior. As shown in Fig. 2c, the QHS plateaus of $n = 5.03 \times 10^{12} \text{ cm}^{-2}$ 2DEG are alternately even, odd and half-integer. As we will clarify in the subsequent paragraphs, the contrasting QHS behavior between 2DHG and 2DEG represent the quantum signatures of rather different band topology between the VB and CB of BAs under \mathbf{E}_z , which split into flavor-dependent D^\pm Rashba valleys and conventional Γ -centered Rashba bands, respectively.

To get insights into the exotic QHS transitions in 2DHG and 2DEG, we have measured R_{xx} and R_{xy} as a function of carrier doping by continuously tuning V_g across the band gap, while keeping the devices at 0.27 K

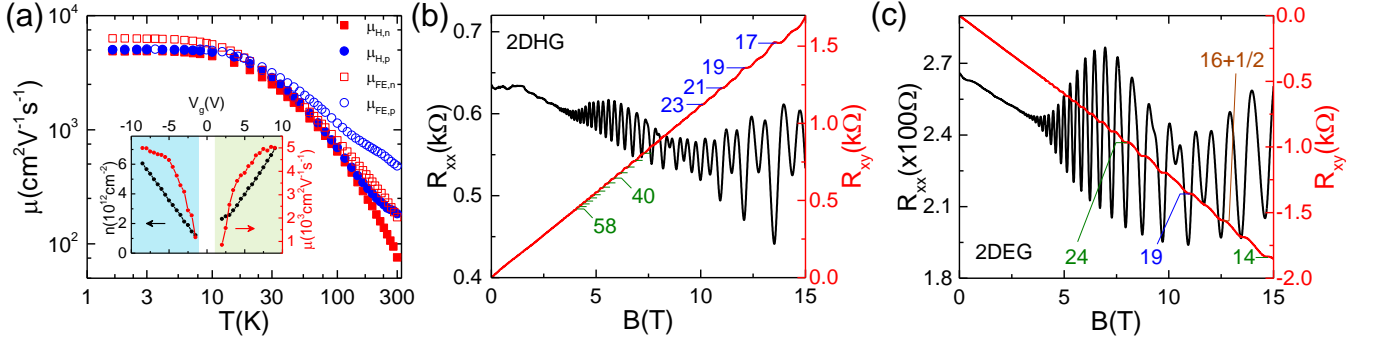


Figure 2. SdH oscillations and quantum Hall states transitions in BAs 2DHG and 2DEG. **a**, T -dependent Hall mobility μ_H measured with $V_g = +7$ V (electron) and $V_g = -7$ V (hole). Inset: Ambipolar FET transfer characteristics at 0.27 K, demonstrating V_g -controlled Fermi level shifting from CB to VB. **b**, *Even-to-odd* QHS transitions in BAs 2DHG with $5.30 \times 10^{12} \text{ cm}^{-2}$ hole doping. **c**, SdH oscillations in BAs 2DEG with $5.03 \times 10^{12} \text{ cm}^{-2}$ electron doping.

and in constant B of 15 T. As shown in Figure 3a, for 2DHG, odd- ν [$\nu = 2n + 1$, where n is the Landau (LL) index] QHS are predominant over the whole doping range, while the lifting of spin degeneracy by magnetic field leads to the formation of Zeeman double peaks centering discernible even- ν ($\nu = 2n$) kinks in R_{xy} . Using these experimental data, we deduce the ratio between cyclotron energy ($E_C = \hbar eB/m^*$, in which \hbar and m^* represent the reduced Plank constant and effective mass respectively) and Zeeman spin-splitting energy ($E_S = g^* \mu_B B$, where g^* and μ_B are the effective Landé g -factor and the Bohr magneton respectively) to be $E_S \approx 0.49 E_C$ (see SI Note 6). Unlike MoS_2 and WSe_2 , both show prominent density dependence in g^* as a result of enhanced electron-electron interaction with lowering doping, E_S in BAs decreases slightly when hole doping changes from $5.66 \times 10^{12} \text{ cm}^{-2}$ ($V_g = -8$ V) to $2.13 \times 10^{12} \text{ cm}^{-2}$ ($V_g = -3$ V), which allows us to exclude the possible origin of the aforementioned *even-to-odd* QHS transitions of 2DHG in the competition of E_C and E_S . Such a claim is also strongly supported by θ -dependent R_{xx} in rotating magnetic field [25], which reveal no significant shifting in Zeeman peaks when B is rotated from 0° to above 60° (See SI Note 6).

Using positive V_g , the density-dependent QHS of 2DEG reveal peculiar transitions in band topology when E_F is tuned in the CB. As shown in Fig. 3a, for $V_g < 5$ V, n -type QHS exhibit the same odd- ν ($2n + 1$) main sequences, while the local R_{xx} valleys of Zeeman double peaks correspond to weaker even ν . For $V_g > 5$ V, QHS are robust for both even and odd filling factors, as evident by $\nu = 11, 12, 13$, and 14 plateaus. Even more strikingly, QHS become half-integer quantized in the form of $\nu' = \nu + 1/2$, for $\nu = 16, 17$, and 18 plateaus. These exotic changes in 2DEG QHS are rooted in the formation of two Γ -centered Rashba bands in the CB, when spin degeneracy are lifted by \mathbf{E}_z -activated SOC. Unlike the protected gapless surface states in topological insulators, the Γ -Rashba band crossing point in BAs is topologically trivial and becomes gapped by external field. At 15 T and 0.27 K, the gapped Γ -Rashba bands can be divided

into three QHS zones, as sketched in Fig. 3b. The first zone is for E_F below the Zeeman gap (E_S), corresponding to low positive V_g when the Fermi surface (FS) is characterized by two elliptical pockets produced by weak Rashba splitting and strong in-plane band anisotropy. When quantized, the LLs of these two isolated Fermi pockets are equivalent to the celebrated flavor-dependent LL spectrum of heavily massive Dirac fermions in MoS_2 , in which QHS plateaus in the vicinity of valley extrema follow $\nu = 2n + 1$ [5]. On the other hand, when E_F is well above the Zeeman gap for large V_g , the FSs form unique inner-outer nested structure by intersecting two helical Rashba bands [16, 26]. Due to the helical spin-momentum locking, a π Berry phase emerges in QHS manifested by $\nu = n + 1/2$, where the half integer is the quantum transport fingerprint of massless fermions in topological materials [15, 27–29]. In between these two zones, V_g pushes E_F right into the gap region, creating one large spin-polarized pocket. The LLs of such a non-degenerate band are characterized by integer ν .

The relation between charge carrier polarity and QHS transitions become more intuitive by 2D mapping of R_{xx} as a function of both V_g and B , in which well-defined even and odd QHS states for different SdH minima are labelled by solid lines and ν indexes (Fig. 3c and 3d). Note that for 2DEG, the horizontal indexing of ν is referring to 15 T, while the vertical ν is determined by SdH oscillations at $V_g = 9$ V. For 2DHG, the *even-to-odd* transitions are located at $\nu = 24$, which defines the lower boundary of odd- ν QHS in Fig. 3c. In contrast, odd- ν QHS are both field- and doping-dependent, and thus distributed extensively over the 2D R_{xx} image of 2DEG (Fig. 3d). The different QHS behavior between 2DHG and 2DEG can not be simply attributed to negligible band asymmetry between the CBM and VBM of the Γ valley (see SI Note 1). Instead, it is the manifestation of collective p_x -orbital selectivity for Rashba SOC and Stark effects, which reverse the VBM energy ordering between the Γ and D^\pm valleys when negative V_g is applied. As depicted in Fig. 1d, the Rashba energy splitting of the D valleys

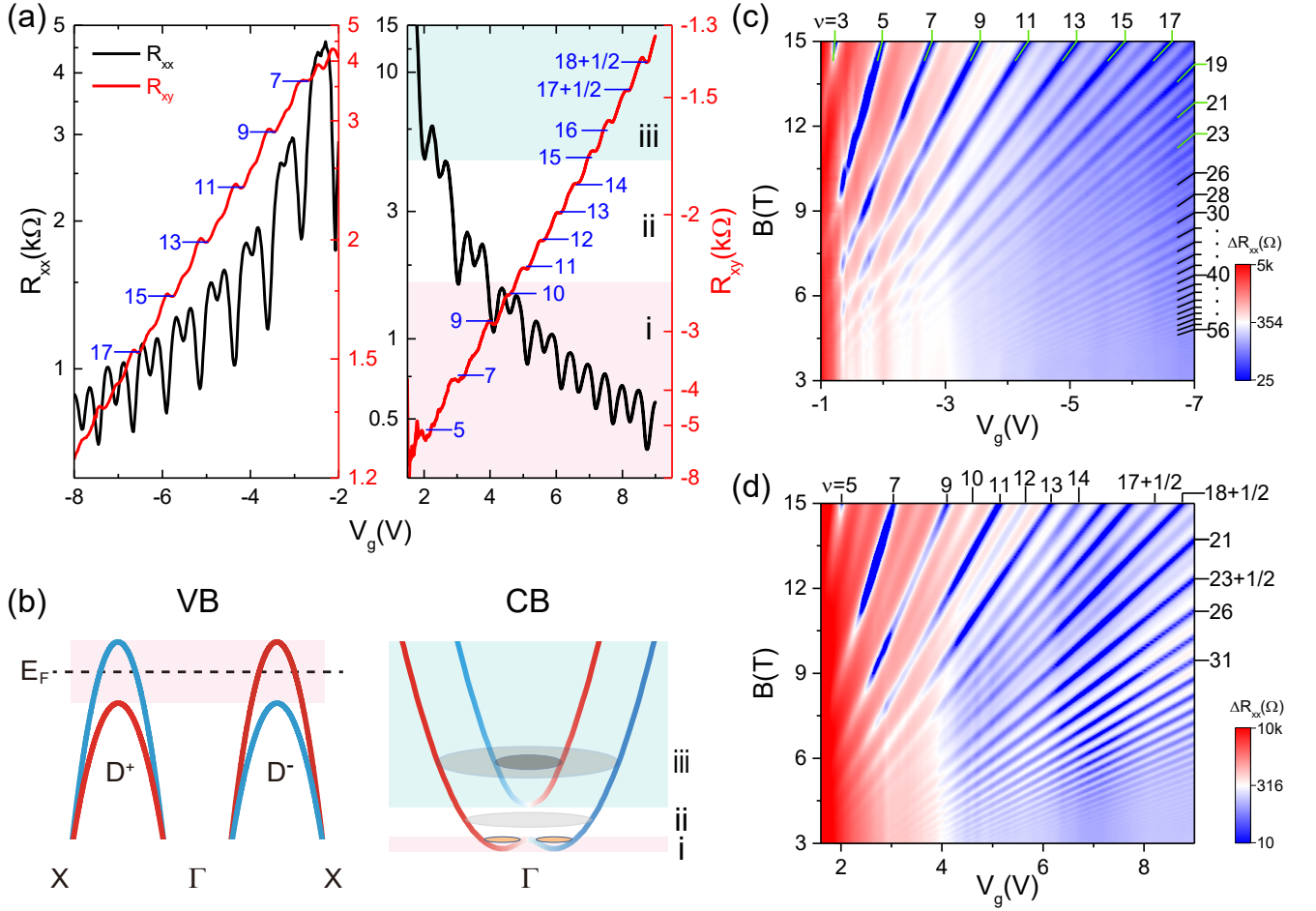


Figure 3. Unconventional quantum Hall signatures of gate-tunable Rashba valley formation in BAs 2DHG and 2DEG. **a**, R_{xx} and R_{xy} as a function of V_g at $B=15$ T and $T=0.27$ K, unfolding all odd- ν QHS sequence for 2DHG but density-dependent transitions in ν from odd, integer to half-integer for 2DEG. **b**, Rashba band formation of the VB and CB of BAs under external electric field. The former forms TRS-paired D^\pm valleys like monolayer TMDCs, while the latter is the well-known Γ -Rashba bands. Note that the Γ -Rashba splitting is exaggerated for clarity. **c**, **d** 2D mapping of R_{xx} versus B and V_g for 2DHG and 2DEG, respectively. The mapping data were collected by V_g sweeping with fixed B , which was increased by steps of 0.1 T for $B \geq 9$ T and 0.05 T for $B < 9$ T.

resembles Zeeman effect, rather distinct from the established Γ -Rashba effect. This is because the momentum-dependent band splitting of the D valleys is referenced to the TRIM points of X , which are local band minima of the top VB band. When viewed in the first BZ, the Rashba-split D^\pm are spin-valley polarized as required by TRS.

The quantization of the spin-valley flavored D^\pm valleys shares exactly the same LL structure as monolayer TMDCs, when Rashba SOC creates two groups of LLs (designated by n_I and n_{II} respectively) by breaking both spin and valley degeneracy. As sketched in Fig. 3b, the classification of LLs for the D^\pm -Rashba valleys are based on *flavors*, *i.e.* the sign of $\tau_z \sigma_z$ (± 1). TRS between the D^+ and D^- valleys enforces double degeneracy in each set of LLs, with the only exception of spin lifted $n_i = 0$ LLs [5]. For low negative V_g , E_F only intersects n_I -group LLs, and ν follows the odd sequences of $2n + 1$ when B

linearly increases LL degeneracy. By increasing V_g , the FS will include both groups of LLs in low field, producing even- ν QHS which will eventually evolve into odd- ν when E_F crosses over $n_{II} = 0$ LL [5]. Note that the spin-up and spin-down Rashba bands of each D^\pm valley are further subjected to Zeeman splitting, which also contributes to the dynamic *even-to-odd* QHS transitions for 2DHG.

It is apparent in Fig. 2b and 2c that the emergence of Rashba-splitting bands in both 2DHG and 2DEG for high doping levels ($> 5 \times 10^{12}$ cm $^{-2}$) are coincident with strong beating patterns in SdH oscillations [30], due to the formation of dual inner-outer FSs with close cross-section areas. However, for lower doping, the Γ - and D -valley associated Rashba bands have dissimilar beating behavior, as a result of rather different FS topology illustrated in Fig. 3b. Typical low-doping SdH beating patterns of 2DHG (BAs-S9) are characterized by large periodicity and weak oscillation frequency splitting after

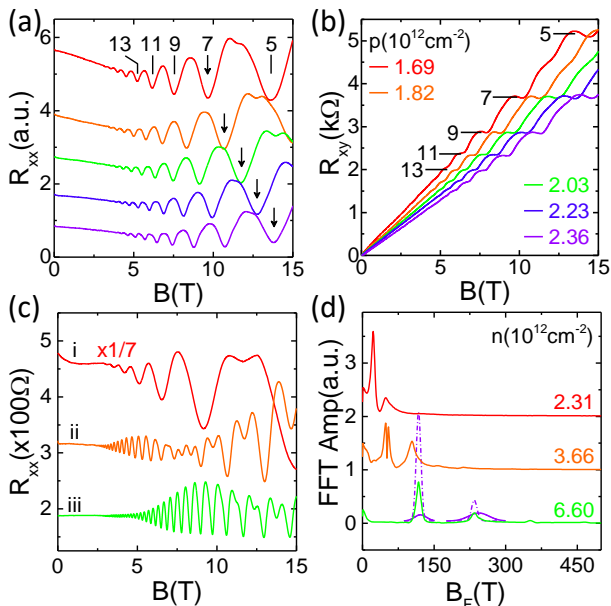


Figure 4. Rashba band splitting controlled SdH beating patterns in BA 2DHG and 2DEG. **a**, In contrast to high hole doping in Fig. 2b, low-doping SdH beating of 2DHG at 0.27 K shows large periodicity and weak FFT frequency splitting. The black arrows indicate the evolution of $\nu = 7$ SdH minima vs hole doping. **b**, QHS plateaus correspond to **a**, showing all odd- ν sequence for low hole doping. **c**, Density-dependent beating patterns in SdH oscillations of 2DEG, which can be divided into three regimes as defined in Fig. 2b. **(d)** The corresponding FFT analyses of **c**, revealing the correlations between FS topology and SdH beating behavior. The superimposed black lines for $6.60 \times 10^{12} \text{ cm}^{-2}$ represent two Gaussian peaks for fitting the beating frequency. Note that the outer-pocket FFT amplitude is multiplied by 3 for clarify.

fast Fourier transform (FFT), in consistent with two well-separate TRS-valley pockets (Fig. 4a and SI Note 4). Because E_F intersects one spin-polarized band for each D valley, the corresponding R_{xy} only shows odd- ν QHS plateaus (Fig. 4b). For 2DEG, the beating patterns are more dynamically evolved as a function of both doping levels and magnetic field (Fig. 4c and 4d). In the vicinity of CBM (Regime-i in Fig. 3b), the SdH beating of 2DEG is also controlled by two spin-polarized Γ -Rashba pockets. By increasing doping and pushing E_F to the Γ Dirac point (Regime-ii in Fig. 3b), the FSs become inner-outer nested, producing strong SdH beating and oscillation frequency splitting. Well above the E_S ($B = 15$ T) gap, two helical Dirac FSs are responsible for strong SdH beating with large periodicity (Regime-iii in Fig. 3b).

The *even-to-odd* transition in QHS of BA 2DHG would be the first experimental demonstration of uncon-

ventional quantum Hall effect of a spin-valley flavored electronic structure [5], which is predicted in monolayer TMDCs but experimentally becomes overshadowed by field- and density-dependent enormous Zeeman effect. The V_g -driven exotic QHS in 2DEG also show the great potential of BA in studying unprecedented gate-tunable quantization phenomena. Considering that B is only 15 T in our experiments, we are expecting to see more fascinating SOC and Rashba related physics in higher magnetic field, such as quantum valley Hall and fractional Quantum Hall effect.

METHODS

BA FET fabrications. During device fabrications, BA/hBN/graphite heterostructures were first assembled by the polycarbonate (PC)-based dry transfer technique [31, 32], which was followed by preparing Au/Pd contacts (60 nm and 2 nm respectively) to BA flakes using standard electron beam lithography. Finally, the top hBN layer was transferred on the top of BA FETs to finish the encapsulation. For micro-mechanical exfoliation, heavily doped silicon substrates with 285 nm SiO_2 were used for good optical contrasts for all three types of 2D crystals used in this study.

Density functional calculations. The first principle calculations of BA were performed using the Vienna *ab initio* package [33] with projector-augmented wave (PAW) [34] pseudopotential and generalized gradient approximation (GGA). For few-layer BA, a 30 Å vacuum layer was adopted to avoid the unphysical interaction. Van der Waals interaction was included by the optB88-vdW exchange functional [35] for band calculations and optimization. During the geometry optimization, the lattice and atomic positions were allowed to relax until the force per atom was smaller than 0.001 eV/Å. The energy cutoff was set to 500 eV and the energy convergence criteria was set to 10^{-6} eV. A Γ -centered $9 \times 10 \times 1$ k -mesh was adopted for all calculations. The effect of spin-orbital coupling (SOC) [36] was included self-consistently due to the considerable SOC energy of 0.43 eV in As. A sawtooth-type periodic potential was applied in perpendicular to the vdW plane to simulate the electric field E_z .

Quantum transport measurements. SdH oscillations and carrier dependent R_{xx} and Hall resistance R_{xy} are measured with two SR830 lock-in amplifiers using a typical excitation current of 100 nA at 13.3 Hz. The gate voltage are supplied by a Keithley 2400. He₃ temperature quantum transport measurements were performed using an HelioxVL insert in a 15-T IntegraAC system (Oxford Instruments). A TeslatronPT cryofree system (Oxford Instruments) was employed to measure angle-dependent and T-dependent R_{xx} and R_{xy} from 1.6 – 300 K.

- [1] Seki, S., Yu, X. Z., Ishiwata, S. & Tokura, Y. Observation of skyrmions in a multiferroic material. *Science* **336**, 198–201 (2012).
- [2] Kimura, T. *et al.* Magnetic control of ferroelectric polarization. *Nature* **426**, 55–58 (2003).
- [3] Bernevig, B. A., Hughes, T. L. & Zhang, S. C. Quantum spin Hall effect and topological phase transition in HgTe quantum wells. *Science* **314**, 1757–1761 (2006).
- [4] Manchon, A., Koo, H. C., Nitta, J., Frolov, S. M. & Duine, R. A. New perspectives for Rashba spin-orbit coupling. *Nat. Mater.* **14**, 871–882 (2015).
- [5] Li, X., Zhang, F. & Niu, Q. Unconventional quantum Hall effect and tunable spin Hall effect in Dirac materials: Application to an isolated MoS₂ trilayer. *Phys. Rev. Lett.* **110**, 066803 (2013).
- [6] Wang, Z. *et al.* Origin and magnitude of ‘designer’ spin-orbit interaction in graphene on semiconducting transition metal dichalcogenides. *Phys. Rev. X* **6**, 041020 (2016).
- [7] Li, L. K. *et al.* Black phosphorus field-effect transistors. *Nat. Nanotechnol.* **9**, 372–377 (2014).
- [8] Xia, F., Wang, H., Hwang, J. C., Castro Neto, A. H. & Yang, L. Black phosphorus and its isoelectronic materials. *Nat. Rev. Phys.* **1**, 306–317 (2019).
- [9] Shportko, K. *et al.* Resonant bonding in crystalline phase-change materials. *Nat. Mater.* **7**, 653–658 (2008).
- [10] Kooi, B. J. & Wuttig, M. Chalcogenides by design: Functionality through metavalent bonding and confinement. *Adv. Mater.* **32**, 1908302 (2020).
- [11] Chen, Y. *et al.* Black arsenic: A layered semiconductor with extreme in-plane anisotropy. *Adv. Mater.* **30**, 1800754 (2018).
- [12] Wang, Z. *et al.* Defects controlled hole doping and multivalley transport in SnSe single crystals. *Nat. Commun.* **9**, 47 (2018).
- [13] Li, L. K. *et al.* Quantum Hall effect in black phosphorus two-dimensional electron system. *Nat. Nanotechnol.* **11**, 592–596 (2016).
- [14] Winkler, R. *Spin-Orbit Coupling Effects in Two-Dimensional Electron and Hole Systems* (Springer-Verlag, Berlin Heidelberg New York, 2003).
- [15] Murakawa, H. *et al.* Detection of Berry’s phase in a bulk Rashba semiconductor. *Science* **342**, 1490–1493 (2013).
- [16] Ishizaka, K. *et al.* Giant Rashba-type spin splitting in bulk BiTeI. *Nat. Mater.* **10**, 521–526 (2011).
- [17] Khoo, K., Mazzoni, M. & Louie, S. Tuning the electronic properties of boron nitride nanotubes with transverse electric fields: A giant DC Stark effect. *Phys. Rev. B* **69**, 201401 (2004).
- [18] Liu, Y. *et al.* Gate-tunable giant Stark effect in few-layer black phosphorus. *Nano Lett.* **17**, 1970–1977 (2017).
- [19] Kim, J. *et al.* Observation of tunable band gap and anisotropic dirac semimetal state in black phosphorus. *Science* **349**, 723–726 (2015).
- [20] Ramasubramaniam, A., Naveh, D. & Towe, E. Tunable band gaps in bilayer transition-metal dichalcogenides. *Phys. Rev. B* **84**, 205325 (2011).
- [21] Clark, A. H. Arsenolamprite confirmed from Copiapo area, northern Chile. *Mineralogical Magazine* **37**, 732 (1970).
- [22] Zhong, M. *et al.* Thickness-dependent carrier transport characteristics of a new 2D elemental semiconductor: Black arsenic. *Adv. Funct. Mater.* **28**, 1802581 (2018).
- [23] Yang, F. Y. *et al.* Quantum Hall effect in electron-doped black phosphorus field-effect transistors. *Nano Lett.* **18**, 6611–6616 (2018).
- [24] Long, G. *et al.* Achieving ultrahigh carrier mobility in two-dimensional hole gas of black phosphorus. *Nano Lett.* **16**, 7768–7773 (2016).
- [25] Xu, S. *et al.* Odd-integer quantum Hall states and giant spin susceptibility in p-type few-layer WSe₂. *Phys. Rev. Lett.* **118**, 067702 (2017).
- [26] Feng, Y. *et al.* Rashba-like spin splitting along three momentum directions in trigonal layered PtBi₂. *Nat. Commun.* **10**, 4765 (2019).
- [27] Novoselov, K. S. *et al.* Two-dimensional gas of massless Dirac fermions in graphene. *Nature* **438**, 197–200 (2005).
- [28] Zhang, Y. B., Tan, Y. W., Stormer, H. L. & Kim, P. Experimental observation of the quantum Hall effect and Berry’s phase in graphene. *Nature* **438**, 201–204 (2005).
- [29] Xu, Y. *et al.* Observation of topological surface state quantum Hall effect in an intrinsic three-dimensional topological insulator. *Nat. Phys.* **10**, 956 (2014).
- [30] Nitta, J., Akazaki, T., Takayanagi, H. & Enoki, T. Gate control of spin-orbit interaction in an inverted In_{0.53}Ga_{0.47}As/In_{0.52}Al_{0.48}As heterostructure. *Phys. Rev. Lett.* **78**, 1335–1338 (1997).
- [31] Wang, L. *et al.* One-dimensional electrical contact to a two-dimensional material. *Science* **342**, 614–617 (2013).
- [32] Zomer, P. J., Guimaraes, M. H. D., Brant, J. C., Tombros, N. & van Wees, B. J. Fast pick up technique for high quality heterostructures of bilayer graphene and hexagonal boron nitride. *Appl. Phys. Lett.* **105**, 013101 (2014).
- [33] Kresse, G. & Furthmüller, J. Efficiency of ab-initio total energy calculations for metals and semiconductors using a plane-wave basis set. *Comp. Mater. Sci.* **6**, 15–50 (1996).
- [34] Kresse, G. & Joubert, D. From ultrasoft pseudopotentials to the projector augmented-wave method. *Phys. Rev. B* **59**, 1758–1775 (1999).
- [35] Klimeš, J., Bowler, D. R. & Michaelides, A. Chemical accuracy for the van der Waals density functional. *J. Phys. Condens. Matter* **22**, 022201 (2009).
- [36] Koelling, D. D. & Harmon, B. N. A technique for relativistic spin-polarised calculations. *J. Phys. C* **10**, 3107 (1977).

ACKNOWLEDGMENTS

This work is supported by the National Key R&D Program of the MOST of China (Grant Nos. 2016YFA0300204, 2017YFA0303002 and 2019YFA0308602), the National Science Foundation of China (Grant Nos. 11790313, 11574264, 11774305 and 61904205), Zhejiang Provincial Natural Science Foundation (Grant No. D19A040001), and the Natural Science Foundation of Hunan Province (Grant No. 2020JJ4677). Q.L.X. acknowledges the funding support

from the Open Research Fund of State Key Laboratory of Pulsed Power Laser Technology. Y.Z. acknowledges the funding support from the Fundamental Research Funds for the Central Universities.

AUTHOR CONTRIBUTIONS

Q.L.X. and Y.Z. initiated and supervised the project. F.S. fabricated BAs devices and carried out all the mea-

surements, assisted by X.K.S. and J.H. C.Q.H and Y.H.L. did the DFT calculations. K.W. and T.T. prepared high-quality boron nitride single crystals. F.S., C.Q.H., Q.L.X. and Y.Z. analysed the data and wrote the paper with inputs from all authors.

COMPETING FINANCIAL INTERESTS:

The authors declare no competing financial interests.